Colloids and Surfaces B: Biointerfaces 205 (2021) 111919

Contents lists available at ScienceDirect

Colloids and Surfaces B: Biointerfaces

journal homepage: www.elsevier.com/locate/colsurfb

Bio-plotted hydrogel scaffold with core and sheath strand-enhancing mechanical and biological properties for tissue regeneration

Ji Min Seok [a,b,1], Jae Eun Jeong [a,1], Sang Jin Lee [a], Seung Hyun Im [a], Jun Hee Lee [a], Wan Doo Kim [a], Kangwon Lee [b,2,*], Su A Park [a,2,*]

[a] Department of Nature-Inspired System and Application, Korea Institute of Machinery and Materials (KIMM), Daejeon, 34103, Republic of Korea
[b] Department of Applied Bioengineering, Graduate School of Convergence Science and Technology, Seoul National University, Seoul, 08826, Republic of Korea

ARTICLE INFO

Keywords:
Bioprinting
Scaffold
Tissue regeneration

ABSTRACT

Three-dimensional bio-plotted scaffolds constructed from encapsulated biomaterials or so-called "bio-inks" have received much attention for tissue regeneration applications, as advances in this technology have enabled more precise control over the scaffold structure. As a base material of bio-ink, sodium alginate (SA) has been used extensively because it provides suitable biocompatibility and printability in terms of creating a biomimetic environment for cell growth, even though it has limited cell-binding moiety and relatively weak mechanical properties. To improve the mechanical and biological properties of SA, herein, we introduce a strategy using hydroxyapatite (HA) nanoparticles and a core/sheath plotting (CSP) process. By characterizing the rheological and chemical properties and printability of SA and SA/HA-blended inks, we successfully fabricated bio-scaffolds using CSP. In particular, the mechanical properties of the scaffold were enhanced with increasing concentrations of HA particles and SA hydrogel. Specifically, HA particles blended with the SA hydrogel of core strands enhanced the biological properties of the scaffold by supporting the sheath part of the strand encapsulating osteoblast-like cells. Based on these results, the proposed scaffold design shows great promise for bone-tissue regeneration and engineering applications.

1. Introduction

Three-dimensional (3D) scaffolds fabricated using additive manufacturing (AM) processes have been widely used in tissue regeneration. These scaffolds can be precisely designed to optimize the rebuilding of an entire injured structure, compared with traditional therapies [1–3]. As one category of AM, 3D plotting (3DP) systems have attracted much attention due to their adaptability to various bio-materials and scaffold specifications for the desired tissue regeneration application [4–6]. Chimene et al. and Donderwinkel et al. showed that 3DP can be applied to the printing of cells encapsulated in bio-materials, with high viscosity and cell density; this process is also known as bio-plotting (BP) [7,8]. As suggested by previous studies, scaffolding fabrication requires control over a variety of BP conditions, such as the base materials used for the ink, the cell type, the printing conditions, and the strand parameters (e.g., strand width, distance between strands, the strand pattern, and the degree of interconnectivity) [9–12].

Non-toxic, biocompatible, and biodegradable polymers are commonly incorporated in bio-inks to promote and preserve cell viability [7,11,13]. As a natural polymer synthesized from brown seaweed with a structure similar to that of native extracellular matrix, sodium alginate (SA) is increasingly used as a base material for bioprinting, due to its versatile properties and ability for ionic cross-linking with Ca^{2+} ions for tunable printability [14,15]. Moreover, the mechanical properties of bio-inks incorporating SA can easily be modified by varying the molecular weight and concentration for stable encapsulation of the cells during printing. However, overall, most hydrogel materials have relatively weak mechanical strength. Additionally, SA is lacking in cell-adhesive moieties for cell attachment [16,17]. To address these issues, SA is commonly blended with other inorganic materials [18–21]. As described in the previous investigations, hydroxyapatite (HA) has been widely used as a bio-ceramic material to improve the mechanical properties and biocompatibility of scaffolds, by enhancing

* Corresponding authors.
E-mail addresses: kangwonlee@snu.ac.kr (K. Lee), psa@kimm.re.kr (S.A. Park).
[1] These co-authors have made equal contributions to this work.
[2] These corresponding authors have made equal contributions to this work.

https://doi.org/10.1016/j.colsurfb.2021.111919
Received 31 March 2021; Received in revised form 6 June 2021; Accepted 8 June 2021
Available online 10 June 2021

the stiffness and bio-mineralization capability for bone tissue repair [22–24].

Core/sheath plotting (CSP) preserves the specific properties of the ink constituents to enhance the printability and scaffold functionality of the 3D structure [25,26]. In brief, CSP extrudes the different materials through the core and sheath parts of the nozzle, creating a dual strand that has a cross-section similar to that of a pencil. Especially, the mechanical support ink and bio-ink can be plotted separately in the core or sheath parts of the nozzle for specific tissue-engineering applications [27]. However, to date, direct BP has been limited by the washing and heat treatments required to remove organic solvents from the polymer suspension housing the active material in the bio-ink, which has a negative effect on the encapsulated cells. To address these issues, we considered a BP process in which various bio-materials can be printed rapidly via CSP to create a bio-scaffold with improved functionality for tissue regeneration.

In this study, we examined the materials and processes used in BP to identify biomaterials or their combination that would synergistically enhance the mechanical integrity and cell viability of printed scaffolds for tissue-engineering applications. SA was used as the base material of the bio-ink. An ink blend created by combining SA and HA was used to enhance the mechanical properties of the scaffold and the biological properties of the bio-ink, as the core and sheath, respectively. Before the plotting process, we attempted to optimize the ink composition through rheological and chemical characterizations as the amounts of SA and HA in the core and sheath were varied. This was followed by a printability test of the ink samples using 3DP. After preparing the inks for plotting, we fabricated scaffolds with the optimized core/sheath strand configurations using CSP. The fabricated scaffolds were examined under mechanical testing. The biological functions of the selected scaffolds were measured in an in-vitro test for bone tissue regeneration with MC-3T3 osteoblast-like cells. Our results show that the proposed CSP method is capable of generating bio-scaffolds with enhanced mechanical and biological properties for bone tissue engineering.

2. Materials & methods

2.1. Preparation of the core and sheath ink

SA (Sigma-Aldrich, St. Louis, MO, USA) and HA (Sigma-Aldrich) powders were placed in vials and dissolved in Dulbecco's modified Eagle's medium (DMEM; HyClone) with 3, 4, and 5 wt% (SA solution) and 0, 10, and 20 wt% (HA solution) with magnetic stirring for 1 h at room temperature. After preparation, the solutions were pre-crosslinked using 1% $CaCl_2$ solution by physical mixing. The SA/HA ratios of the ink blends are listed in Table 1 with abbreviations to denote the makeup of individual ink/blended ink specimens. For example, A3H0, A4H0, and A5H0 correspond to an ink with 3, 4, and 5 wt% SA and 0% HA, respectively, with "A" denoting SA and "H" denoting HA followed by the content percentage of each.

MC-3T3 osteoblast-like cells were used in the preparation of the sheath ink for bone tissue regeneration by being cultured in DMEM with 10% fetal bovine serum (FBS; CellSera, Rutherford, New South Wales, Australia) and 1% penicillin-streptomycin (10,000 units/mL penicillin and 10 mg/mL streptomycin, Gibco Laboratory, Gaithersburg, MD, USA). The cells were cultured with approximately 80 % confluence on a dish in an incubator with 5% CO_2 at 37 °C. After the cell culture was complete, we prepared the cell suspension by gently pipetting in DMEM to create a cell density in the bio-ink of 3×10^6 cells/mL. The cell suspension was then mixed with SA solution (3 wt%) and pre-crosslinked using 1% $CaCl_2$ solution with the core ink.

Table 1
Acronyms of the sodium alginate (SA) and hydroxyapatite (HA) inks.

Acronyms	Sodium alginate (SA) powder		
	3 wt%	4 wt%	5 wt%
Hydroxyapatite (HA) solution			
0%	3A0H	4A0H	5A0H
10 %	3A10H	4A10H	5A10H
20 %	3A20H	4A20H	5A20H

2.2. Characterization of the core and sheath ink

The viscosities of the inks were examined over a shear rate range of 0.01–100 s^{-1} in a rheometer (Kinexus Lab+, Malvern/Netzsch, Selb, Germany). The storage moduli of the inks were determined with a frequency sweep experiment over a frequency range of 0.1–10 Hz. In addition, all samples of both tests were evaluated in terms of a cone/plate geometry, with a gap of 1 mm at room temperature. The scaffold composition was analyzed using Fourier-transform infrared spectroscopy (FTIR; Alpha, Bruker Corp., Billerica, MA, USA) over the range of 4000 to 400 cm^{-1} at a resolution of 2 cm^{-1}.

The prepared inks were printed using a custom-designed laboratory 3DP system (in the Korea Institute of Machinery and Materials). The 3DP process was described in a previous study [17]; briefly, this system controls the plotting temperature, pressure, and velocity of the printing head, as well as the plate. The system is capable of precise movements in a rectangular coordinate system, with layer-by-layer stacking functionality for scaffold fabrication. This system was used to test the printability of individual and blended inks by controlling the pneumatic conditions over a range of 0–500 kPa in 10 units, using the dispensing machine of the 3DP system. During the printability test, the syringe gauge and velocity remained fixed at 21 G and 300 mm/min, respectively.

2.3. Fabrication and characterization of the scaffold

After the printability test using all prepared inks, the scaffolds were fabricated using selected inks that could be extruded stably as a strand. Based on the printability of the core inks, we fabricated the scaffold using the CSP process with a dual concentric nozzle (inner diameters: 500/400 μm). The plotting velocity and syringe gauge were the same as those used in the core printing test, and the pneumatic/pressure conditions of the sheath were held constant for all prepared bio-inks. After plotting the scaffolds, crosslinking was conducted in a 5% $CaCl_2$ solution over a period of a few minutes. The scaffolds were then cultured in an incubator with 5% CO_2 at 37 °C.

The connected morphology of the core and sheath strands was measured by scanning electron microscopy (SEM; TOPCON Co. Ltd., Tokyo, Japan). To obtain SEM images, the scaffold was lyophilized at −85 °C for 12 h using a freeze-dryer (Il Shin Biobase Co. Ltd, Gyeonggi-do, Korea). Then, the scaffolds were sputter-coated with platinum for 2 min at 30 mA.

The mechanical properties of the scaffolds were manually measured in compression mode using a mechanical testing machine (EZ Test, Shimadzu Corp., Kyoto, Japan). The compressive strength of the scaffolds (size: $7 \times 7 \times 5$ mm^3, $n = 3$) was recorded at a rate of 5 mm/min with a 0.4-kN load cell. The scaffolds were measured in the wet state.

2.4. In-vitro test of the scaffold

The cell viability of the bio-plotted scaffolds was measured using a live/dead cell assay kit (Life Technologies Corp., Carlsbad, CA, USA) over a 7-day period. Calcein AM and ethidium homodimer-1 (EthD-1) were used to stain live (green) and dead (red) cells on the scaffold for 30 min in an incubator, based on the manufacturer's instructions. After staining, the scaffolds were washed using 1X phosphate buffered saline (PBS, HyClone Laboratories, Logan, UT, USA). The scaffolds were then imaged with a fluorescence microscope (ECLIPSE-Ti, Nikon Corp., Tokyo, Japan). To evaluate the cell proliferation and viability, we used the WST-1 cell proliferation assay (Takara Bio, Shiga, Japan) according to the manufacturer's instructions; the evaluation took place over a

period of 7 days. Briefly, WST-1 solution (10 v/v%) was mixed with DMEM, and then, the scaffolds were incubated with the mixed solution for 30 min. After incubation of the scaffold, the absorbance of the medium at 450 nm was measured using a microplate reader (Bio-Rad Laboratories, Hercules, CA, USA). The osteogenic differentiation of the MC-3T3 cells in the scaffolds was evaluated using an alkaline phosphatase (ALP) assay kit (Takara). Here, the scaffold-encapsulated cells were immersed in filtered 0.5 M ethylenediaminetetraacetic acid (EDTA; Invitrogen, Carlsbad, CA, USA) to dissolve the alginate hydrogel, and the solution was centrifuged for 3 min at 1300 rpm using a centrifuge (MF550, Hanil Scientific, Gimpo, Korea). The supernatants were removed, and the cell pellets were washed with PBS. Then, the cell suspensions were centrifuged under the same conditions as before, and the supernatants were removed. To obtain cell lysate, 400 μL of radioimmunoprecipitation assay buffer (RIPA buffer; Thermo Fisher Scientific, Waltham, MA, USA) was added to the cells. After freeze-thawing, the cell lysate was sonicated (5 min, 117 W) and centrifuged using a micro centrifuge (MIKRO 200, Hettich, Beverly, MA, USA) at 4 °C to remove cell debris. The supernatants were placed in a 96-well plate, and para-nitrophenyl phosphate (p-NPP) substrate solution was added at a 1:1 ratio to the solution. After incubation for 1 h at 37 °C, a stop solution (0.5 N NaOH) was added to each well, and the absorbance was measured at 405 nm using a multi-mode microplate reader (SpectraMax iD3, Molecular Devices LLC, San Jose, CA, USA). Finally, a DNA assay was performed using a PicoGreen dsDNA assay kit (Molecular Probes Inc., Eugene, OR, USA), according to the manufacturer's protocol to normalize ALP activity.

2.5. Statistical analysis

All experiments were performed in triplicate; values are presented as the mean ± standard deviation (SD). Statistical analysis was performed using one-way analysis of variance with Tukey's post hoc test. P-values of less than 0.05 were considered statistically significant.

3. Results & discussion

3.1. Characterization of the core and sheath ink

3.1.1. Rheological properties

The viscosity of the ink is a crucial parameter with regard to stable plotting at the microscale for structural fidelity; additionally, the ink viscosity affects the viability and proliferation of the encapsulated cells in terms of the resulting stiffness of the structure [12,28]. Accordingly, we varied the viscosity of the ink by changing the weight ratio of SA and HA. Fig. 1(a) shows the viscosities of 3A0H, 4A0H, and 5A0H (notably inks with SA only) of 790.5, 1967, and 3486 Pa·s, respectively, at a shear rate of 0.1 s^{-1}. Moreover, when HA was added to the inks to create blended SA/HA inks as 3A10H, 4A10H, and 5A10H (3, 4, and 5 wt% SA with 10 % HA, respectively), viscosities of 1343, 2818, and 5712 Pa·s, respectively, were resolved. Increasing the HA content to 20 % in samples 3A20H, 4A20H, and 5A20H resulted in viscosities of 1882, 4254, and 6988 Pa·s, respectively, at a shear rate of 0.1 s^{-1}. Additionally, as shown in Fig. 1(b), we evaluated the storage and loss moduli for characterization of the viscoelastic properties of the inks. The viscosity and moduli of the inks increased with the SA and HA concentrations. In particular, the higher the HA content, the higher the viscosity of the ink,

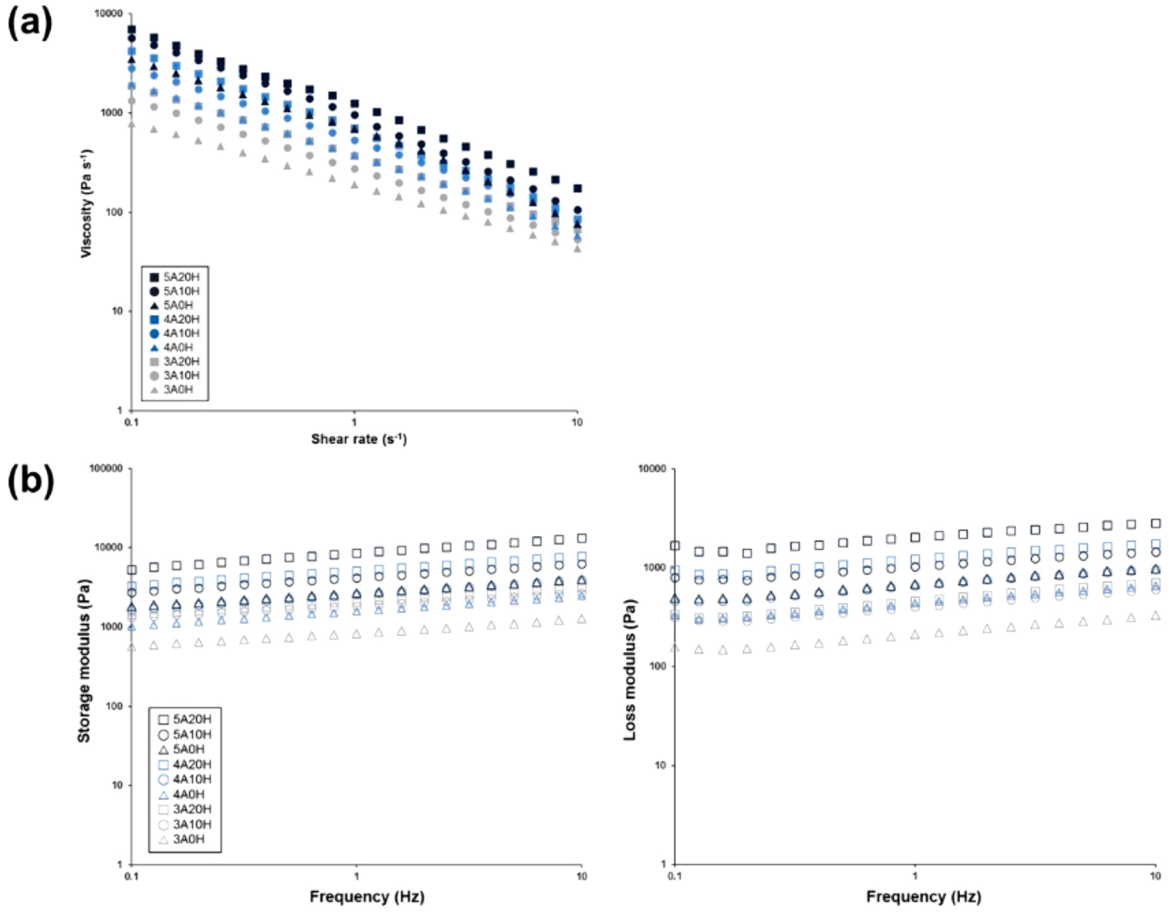

Fig. 1. Rheological properties of the core part ink: (a) viscosity variation with respect to the shear rate and (b) storage and loss moduli behavior as a function of the frequency.

implying that the viscosity could be increased simply by customizing the mix ratio, despite the many variables that could potentially be optimized (e.g., particle size and dispersion degree). The shear thinning shape for suitable plotting is shown in the graph of Fig. 1(a) over all groups [8]. Taken together, these results imply that HA enhances the mechanical properties of the ink; thus, we examined the effects of varying the SA concentration in the inks.

3.1.2. Chemical composition

The chemical compositions of SA and HA in the inks were measured using FT-IR analysis. The negative charge of carboxylate in SA has a tendency to form a complex with HA particles to stabilize the chemical composition [29]. Fig. 2 shows all inks with characteristic SA peaks confirmed at 1409 and 1594 cm^{-1} corresponding to the COO^- group and CO— bond, respectively. The peaks observed between 3400 and 3200 cm^{-1} were identified as the OH stretching vibration of SA [30]. In the spectra, 1022, 605, and 565 cm^{-1} features were associated with phosphate groups in SA/HA blended inks (3A10H, 3A20H, 4A10H, 4A20H, 5A10H, and 5A20 H) [31]. In particular, C—OC— stretching at 1027 cm^{-1} was observed in the inks containing SA only (3A0H, 4A0H, and 5A0H). As a result, we speculated that the spectrum shift from 1027 to 1022 cm^{-1} when HA was blended with SA indicated successful interaction between the C—OC— bond in SA and Ca^{2+} in HA [29]. Moreover, it was confirmed that SA/HA blended inks retained the original properties of the two inks individually. We then evaluated the printability of the prepared SA/HA blended inks.

3.1.3. Printability

The printability of the ink is considered an important parameter for 3D printing of various biomaterials [2,11]. In this study, printability was assessed by examining the filament deformation in the *x-y* plane of SA and SA/HA blended ink filaments as a function of the pneumatic conditions. The state of the filament was categorized as having formed from an unstable flow, a stable flow, or an over flow, as shown in Fig. 3(a). Unstable flow refers to a disconnection in one filament such that it fails to form a single line; over flow refers to inks that were plotted in excess, such that there were connections between filaments creating gaps for a more porous structure. Stable flow refers to that which maintained the shape fidelity of the scaffold, with no evidence of unstable flow or over flow. From this starting point, we attempted to optimize the stable flow of the ink (Fig. 3(b)). Stable flow was obtained with pressures of 110, 140, and 210 kPa using a plotting velocity of 300 mm/min with samples 3A0H, 3A10H, and 3A20H, respectively; similar tendencies were observed using different SA concentrations. Plotting pressures of 180, 220, and 260 kPa were able to extrude 4A0H, 4A10H, and 4A20H samples, respectively; 5A0H, 5A10H, and 5A20H were plotted at pressures of 250, 360, and 430 kPa, respectively. Notably, the printing pressure increased with the SA and HA concentrations, in accordance with the rheological properties of the materials. As the HA content continued to increase, the plotting became less stable; we speculate that this may have been due to the aggregation of HA particles. Thus, the weight ratio of HA did not exceed 20 %. Accordingly, based on the plotted SA/HA blended inks using 3D printing, we fabricated scaffolds having a core/sheath structure using CSP.

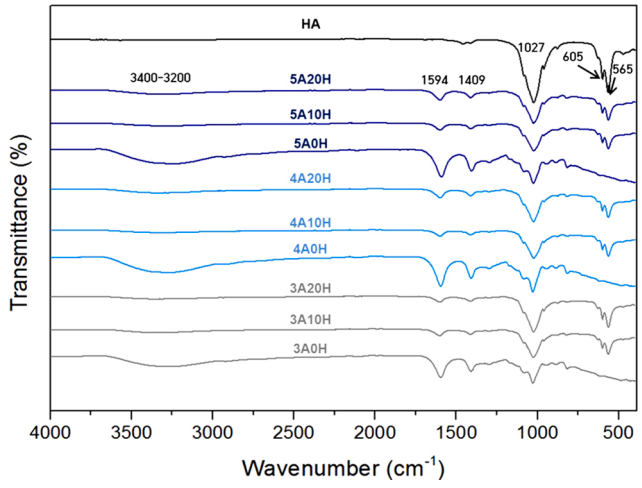

Fig. 2. Fourier-transform infrared spectra of various concentrations of sodium alginate (SA)/hydroxyapatite (HA) blended inks.

3.2. Fabrication and characterization of the scaffold

Scaffolds with core and sheath strands were fabricated using CSP after an investigation of the rheological and chemical properties and the printability of the SA/HA inks. As shown in Fig. 4(a), the entire scaffold size was 20 × 20 mm^2, with eight layers stacked; the strand size was 1.4 mm before post-crosslinking. CSP promotes cell proliferation and differentiation by facilitating nutrient and waste exchange in an optimal substrate for growth [1,32]. Fig. 4(b) shows that the core and sheath were successfully connected, as the HA particles settled stably in SA according to their content. In our fabrication method, there were no harmful organic solvents involved in crosslinking SA in the core and sheath parts, with the exception of the $CaCl_2$ solution. Additionally, the CSP process took only a few minutes with MC-3T3 osteoblast-like cells in the sheath part of the ink. By implementing the core and sheath strand, we anticipated that the mechanical and osteogenic properties of the blended scaffolds would be improved compared to scaffolds produced using SA ink only [33].

The mechanical properties of the scaffolds were measured under compression testing using a universal testing machine (UTM). As a crucial parameter to provide an optimal substrate for bone tissue regeneration, the mechanical properties of the scaffold should be designed using a biomaterial that is similar to bone tissue. As a main constituent of bone, HA has been used extensively as the primary material to mechanically support hydrogels for bone tissue engineering applications [22–24]. Therefore, we fabricated the scaffold with SA- and HA-blended parts to mechanically support the strands plotted using SA bio-ink encapsulating the cells. Mechanical tests of the scaffolds were performed to determine their compressive strengths. The compressive strength results are shown in Fig. 5. In brief, the mechanical strength increased with the concentrations of SA and HA. The compressive strength of the scaffold showed a relative increase of up to 87.9 % in the case of the 5A20H group compared with the 3A0H (SA only) scaffold as a control group. As a result, we successfully created a scaffold fabricating platform for tissue regeneration in a short time using CSP. The platform is capable of extruding a blended hydrogel composite with bio-ceramics and is sufficiently robust for the repair of defective tissue owing to its similar chemical composition to that of bone tissue. We anticipate that this mechanically improved hydrogel scaffold could aid in bone regeneration by mimicking the extracellular matrix [34]. Accordingly, the bioactivity of the scaffold was confirmed in in-vitro tests using 5A0H, 5A10H, and 5A20H scaffolds, which were selected for their relatively high mechanical strength compared with the other ink samples.

3.3. In-vitro test of the scaffold

SA has been widely used as a matrix to stably hold cells due to its structural similarity to the extracellular matrix and its hydrophilic nature. In this study, the SA-only (0% HA content) scaffolds served as a control regarding the gelation degree of the scaffolds and their ability to be adjusted in terms of their ionic interaction for optimal printability and enhanced mechanical strength [11,35]. However, SA is lacking in bioactivity due to having an insufficient number of sites for cell attachment; additionally, it lacks the strength to maintain the necessary scaffold structure [36]. Therefore, as a bioceramic for repairing defective tissue, HA was blended with SA to enhance its affinity for cell

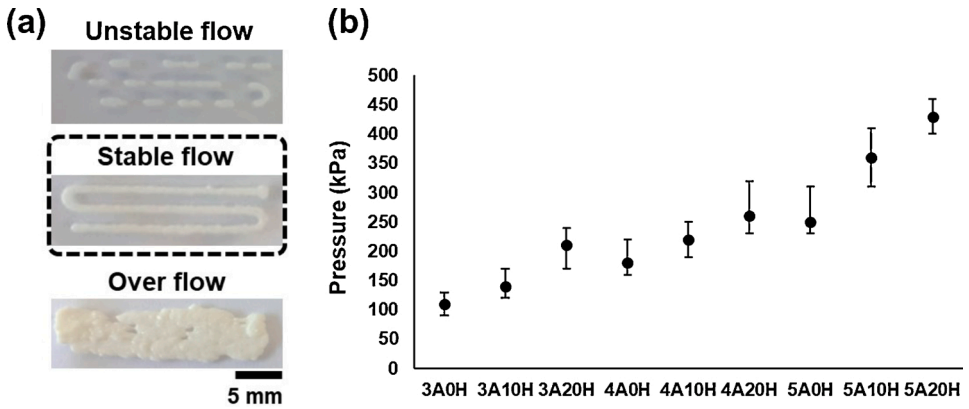

Fig. 3. Printability of the ink: (a) optical images of the printability under unstable, stable, and overflow conditions and (b) pneumatic pressure with stable flow for each group with 3, 4, or 5 wt% SA and/or 0, 10, or 20 % HA content (e.g., "3A0H" refers to 3 wt% SA and 0% HA and so on).

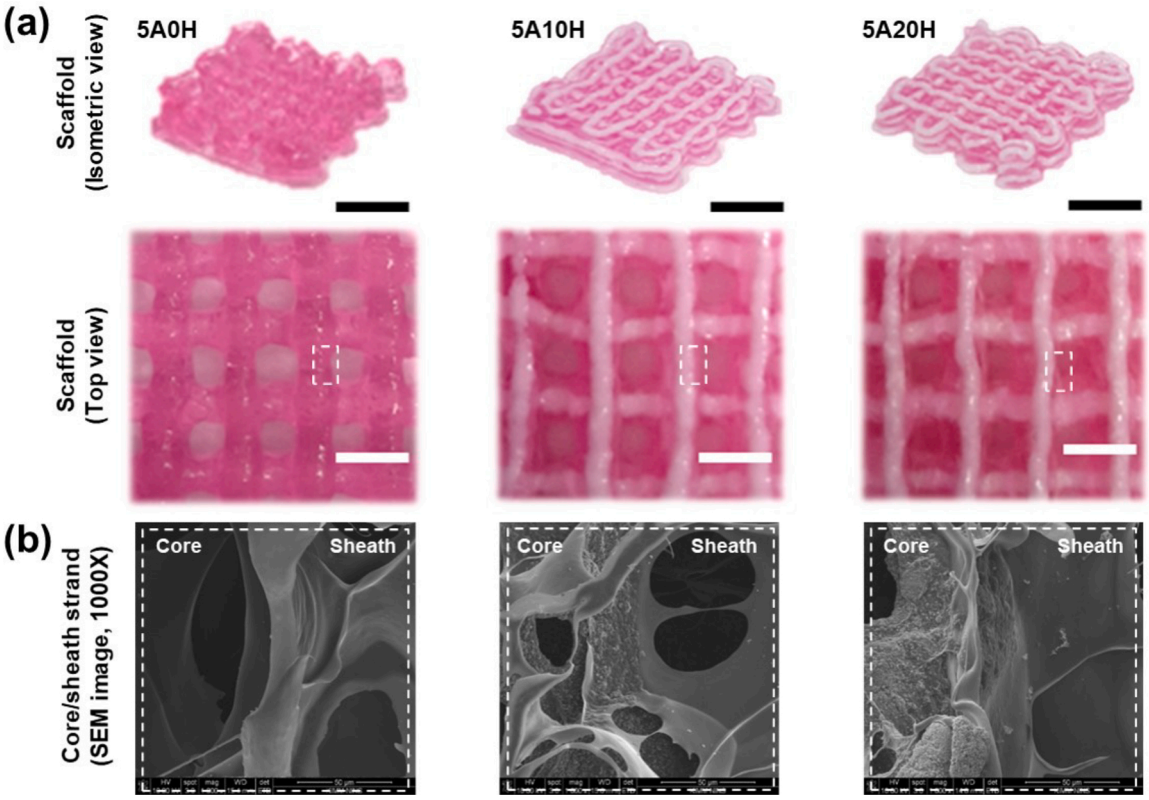

Fig. 4. Images of the core/sheath scaffold: (a) optical images of the scaffold in isometric view and top view, (b) scanning electron microscopy images of the core/sheath strand cross-section in the lyophilized scaffold [scale bars: black = 10 mm; white = 5 mm].

proliferation and osteogenic differentiation [37]. Based on the characterization of the inks and scaffolds, the viability and distribution of MC-3T3 cells encapsulated in the sheath part of the scaffold were measured using a live/dead assay over a 7-day period.

Fig. 6 shows that the cells were well distributed throughout the scaffold, with a relatively small number of dead cells in the structures of the core and sheath strands over the 7-day timeframe. As shown for day 7 in the 5A10H and 5A20H scaffolds, cells were readily observed at the periphery of the core strand. Results from the viability assay indicated that the HA in the core strand improved the biocompatibility of the scaffold. Further analysis of the proliferation and osteogenic differentiation of osteoblast-like cells was conducted using WST-1 and ALP assays, respectively. As shown in Fig. 7(a), the metabolic activity of the cells increased with HA content on day 1. In particular, the initial cell density of the bio-ink in the sheath area was 3×10^6 cells/mL, which was the same density in all groups. Moreover, the activity increased slightly with HA content in the core part, although no significant difference was observed between the 5A0H scaffold and other scaffold types at day 7. This indicates that HA particles promote cell adhesion and migration from the sheath strand encapsulating cells to the core strand consisting of SA and HA ink [24].

ALP analysis was performed to determine the osteogenic differentiation of the cells in the scaffolds (Fig. 7(b)). Cells were extracted after 14 days of scaffold incubation. The results showed that the ALP activity increased significantly with HA content in the core strand. Especially, the 5A20H scaffold with the highest HA content showed higher ALP activity than the other groups. As the HA ratio increased, the ALP activity between the groups was about 1.5 times higher. Thus, the HA

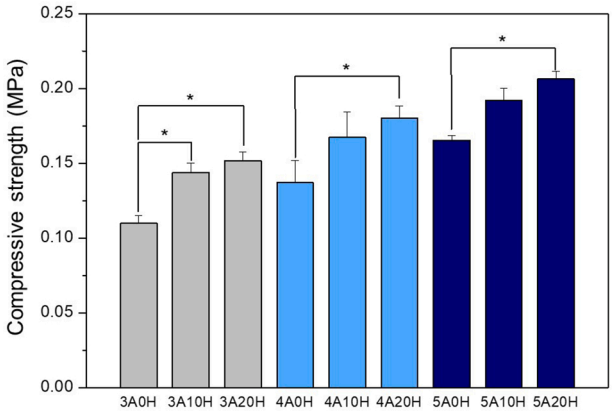

Fig. 5. Compressive strength of the core/sheath scaffold under wet conditions [n = 3, *p < 0.05].

particles in the core strand enhanced osteogenic differentiation, as well as the proliferation of osteoblast-like cells [33]. In particular, the attachment of MC-3T3 cells was promoted by core strands consisting of both SA and HA [38]. Moreover, there is considerable flexibility in the design of the scaffold features to suit various tissue engineering applications, given that the SA hydrogel in the strands can easily be varied to meet the desired mechanical and biological specifications [35,39]. Based on these results, we speculate that the complementary role and structure of the SA/HA blended ink core/sheath strands allow for optimal functionality in the resulting scaffolds, which in turn promotes the bioactivity of cells in the scaffold.

4. Conclusions

In this study, we developed a structure consisting of core and sheath strands as a mechanical and biological support and encapsulation structure of osteoblast-like cells, respectively. In particular, the core and sheath strands of the scaffold were stably crosslinked by the ionic interaction with SA and the divalent ions and HA. The mechanical properties of the scaffold were regulated by the SA and HA

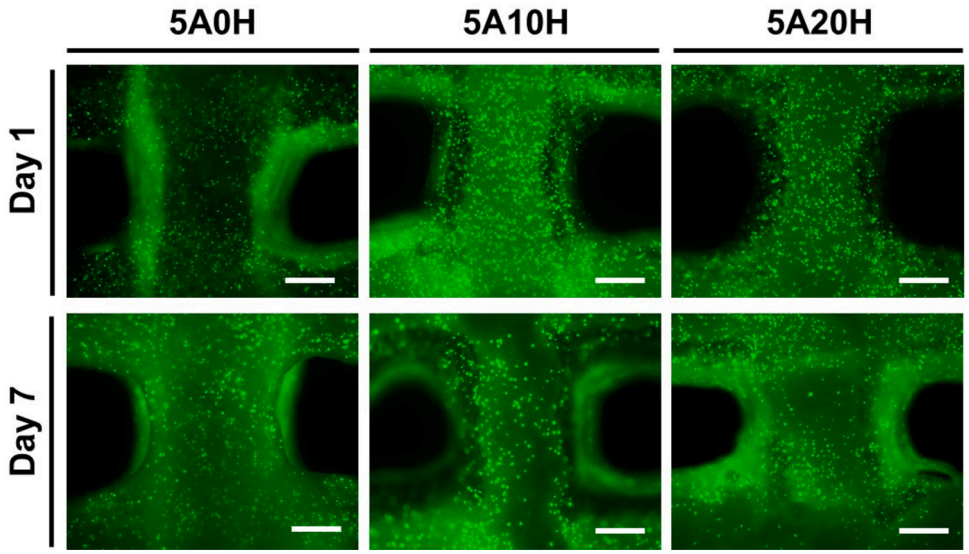

Fig. 6. Fluorescence microscopy images of the core/sheath scaffold after 1 day and 7 days of incubation (scale bar =500 μm).

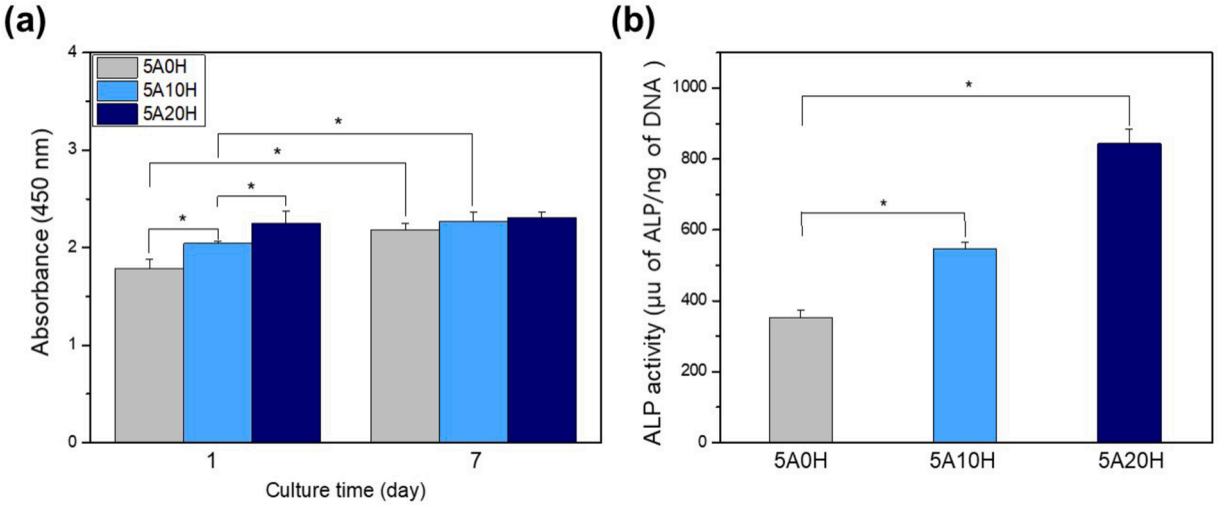

Fig. 7. Cell proliferation and differentiation of MC3T3-E1 in the core/sheath scaffold: (a) WST-1 assay for cell proliferation in the scaffold after 1 day and 7 days of incubation, (b) quantitative analysis of alkaline phosphatase (ALP) activity of pre-osteoblast cells after 14 days of incubation [n = 3, *p < 0.05].

concentrations. Higher rheological properties and compressive strength were achieved using inks consisting of an SA/HA blend than one with SA alone. Cell viability, proliferation, and osteogenic differentiation of osteoblast-like cells increased with the SA and HA concentrations of the scaffolds, compared to those using only SA. Thus, scaffolds created with core and sheath strands consisting of both SA and HA showed enhanced mechanical strength and cell bioactivity, suggesting the suitability of this scaffold construction for bone tissue regeneration and engineering applications. In further, we could consider to the novel combination of various natural and synthetic biomaterials that can simultaneously improve printability and cell culture.

CRediT authorship contribution statement

Ji Min Seok: Writing - original draft, Conceptualization. **Jae Eun Jeong:** Writing - original draft, Methodology. **Sang Jin Lee:** Methodology, Formal analysis. **Seung Hyun Im:** Methodology, Formal analysis. **Jun Hee Lee:** Investigation, Resources. **Wan Doo Kim:** Investigation, Resources. **Kangwon Lee:** Supervision. **Su A Park:** Writing - review & editing, Supervision.

Declaration of Competing Interest

There are no conflicts to declare.

Acknowledgment

This research was supported by the National Research Foundation (NRF) funded by the Korean government (MSIT; No. NRF-2019M3A9E2066348 and 2020M3H4A1A02084828).

References

[1] S.J. Hollister, Porous scaffold design for tissue engineering, Nat. Mater. 4 (2005) 518–524, https://doi.org/10.1038/nmat1421.
[2] S.V. Murphy, A. Atala, 3D bioprinting of tissues and organs, Nat. Biotechnol. 32 (2014) 773–785, https://doi.org/10.1038/nbt.2958.
[3] Y. Luo, X. Wei, Y. Wan, X. Lin, Z. Wang, P. Huang, 3D printing of hydrogel scaffolds for future application in photothermal therapy of breast cancer and tissue repair, Acta Biomater. 92 (2019) 37–47, https://doi.org/10.1016/j.actbio.2019.05.039.
[4] K. Schütz, A.M. Placht, B. Paul, S. Brüggemeier, M. Gelinsky, A. Lode, Three-dimensional plotting of a cell-laden alginate/methylcellulose blend: towards biofabrication of tissue engineering constructs with clinically relevant dimensions, J. Tissue Eng. Regen. Med. 11 (2017) 1574–1587, https://doi.org/10.1002/term.2058.
[5] Y. Luo, Y. Li, X. Qin, Q. Wa, 3D printing of concentrated alginate/gelatin scaffolds with homogeneous nano apatite coating for bone tissue engineering, Mater. Des. 146 (2018) 12–19, https://doi.org/10.1016/j.matdes.2018.03.002.
[6] T.S. Jang, H. Do Jung, H.M. Pan, W.T. Han, S. Chen, J. Song, 3D printing of hydrogel composite systems: recent advances in technology for tissue engineering, Int. J. Bioprinting. 4 (2018), https://doi.org/10.18063/IJB.v4i1.126.
[7] D. Chimene, K.K. Lennox, R.R. Kaunas, A.K. Gaharwar, Advanced bioinks for 3D printing: a materials science perspective, Ann. Biomed. Eng. 44 (2016) 2090–2102, https://doi.org/10.1007/s10439-016-1638-y.
[8] I. Donderwinkel, J.C.M. Van Hest, N.R. Cameron, Bio-inks for 3D bioprinting: recent advances and future prospects, Polym. Chem. 8 (2017) 4451–4471, https://doi.org/10.1039/c7py00826k.
[9] J. Henkel, D.W. Hutmacher, Design and fabrication of scaffold-based tissue engineering, Bio. Nano. Mater. 14 (2013) 171–193, https://doi.org/10.1515/bnm-2013-0021.
[10] C.S. Jung, B.K. Kim, J. Lee, B.H. Min, S.H. Park, Development of printable natural cartilage matrix bioink for 3D printing of irregular tissue shape, Tissue Eng. Regen. Med. 15 (2018) 155–162, https://doi.org/10.1007/s13770-017-0104-8.
[11] J.H.Y. Chung, S. Naficy, Z. Yue, R. Kapsa, A. Quigley, S.E. Moulton, G.G. Wallace, Bio-ink properties and printability for extrusion printing living cells, Biomater. Sci. 1 (2013) 763–773, https://doi.org/10.1039/c3bm00012e.
[12] K. Hölzl, S. Lin, L. Tytgat, S. Van Vlierberghe, L. Gu, A. Ovsianikov, Bioink properties before, during and after 3D bioprinting, Biofabrication 8 (2016), https://doi.org/10.1088/1758-5090/8/3/032002.
[13] Z. Li, S. Huang, Y. Liu, B. Yao, T. Hu, H. Shi, J. Xie, X. Fu, Tuning alginate-gelatin bioink properties by varying solvent and their impact on stem cell behavior, Sci. Rep. 8 (2018), https://doi.org/10.1038/s41598-018-26407-3.
[14] E. Axpe, M.L. Oyen, Applications of alginate-based bioinks in 3D bioprinting, Int. J. Mol. Sci. 17 (2016), https://doi.org/10.3390/ijms17121976.
[15] F.E. Freeman, D.J. Kelly, Tuning alginate bioink stiffness and composition for controlled growth factor delivery and to spatially direct MSC Fate within bioprinted tissues, Sci. Rep. 7 (2017), https://doi.org/10.1038/s41598-017-17286-1.
[16] K.Y. Lee, D.J. Mooney, Alginate: properties and biomedical applications, Prog. Polym. Sci. 37 (2012) 106–126, https://doi.org/10.1016/j.progpolymsci.2011.06.003.
[17] J. Park, S.J. Lee, S. Chung, J.H. Lee, W.D. Kim, J.Y. Lee, S.A. Park, Cell-laden 3D bioprinting hydrogel matrix depending on different compositions for soft tissue engineering: characterization and evaluation, Mater. Sci. Eng. C. 71 (2017) 678–684, https://doi.org/10.1016/j.msec.2016.10.069.
[18] R. Yunus Basha, S.K. Sampath, M. Doble, Design of biocomposite materials for bone tissue regeneration, Mater. Sci. Eng. C. 57 (2015) 452–463, https://doi.org/10.1016/j.msec.2015.07.016.
[19] G. Tozzi, A. De Mori, A. Oliveira, M. Roldo, Composite hydrogels for bone regeneration, Materials (Basel). 9 (2016), https://doi.org/10.3390/ma9040267.
[20] S. Preethi Soundarya, A. Haritha Menon, S. Viji Chandran, N. Selvamurugan, Bone tissue engineering: scaffold preparation using chitosan and other biomaterials with different design and fabrication techniques, Int. J. Biol. Macromol. 119 (2018) 1228–1239, https://doi.org/10.1016/j.ijbiomac.2018.08.056.
[21] H. Goodarzi, S. Hashemi-Najafabadi, N. Baheiraei, F. Bagheri, Preparation and characterization of nanocomposite scaffolds (Collagen/β-TCP/SrO) for bone tissue engineering, Tissue Eng. Regen. Med. 16 (2019) 237–251, https://doi.org/10.1007/s13770-019-00184-0.
[22] G. Wei, P.X. Ma, Structure and properties of nano-hydroxyapatite/polymer composite scaffolds for bone tissue engineering, Biomaterials 25 (2004) 4749–4757, https://doi.org/10.1016/j.biomaterials.2003.12.005.
[23] M. Swetha, K. Sahithi, A. Moorthi, N. Srinivasan, K. Ramasamy, N. Selvamurugan, Biocomposites containing natural polymers and hydroxyapatite for bone tissue engineering, Int. J. Biol. Macromol. 47 (2010) 1–4, https://doi.org/10.1016/j.ijbiomac.2010.03.015.
[24] H. Zhou, J. Lee, Nanoscale hydroxyapatite particles for bone tissue engineering, Acta Biomater. 7 (2011) 2769–2781, https://doi.org/10.1016/j.actbio.2011.03.019.
[25] M.G. Yeo, J.S. Lee, W. Chun, G.H. Kim, An Innovative Collagen-Based Cell-Printing Method for Obtaining Human Adipose Stem Cell-Laden Structures Consisting of Core-Sheath Structures for Tissue Engineering, Biomacromolecules 17 (2016) 1365–1375, https://doi.org/10.1021/acs.biomac.5b01764.
[26] W. Kim, H.S. Yun, G. Kim, An innovative cell-laden α-TCP/collagen scaffold fabricated using a two-step printing process for potential application in regenerating hard tissues, Sci. Rep. 7 (2017), https://doi.org/10.1038/s41598-017-03455-9.
[27] W. Kim, H. Lee, Y. Kim, C.H. Choi, D. Lee, H. Hwang, G. Kim, Versatile design of hydrogel-based scaffolds with manipulated pore structure for hard-tissue regeneration, Biomed. Mater. 11 (2016), https://doi.org/10.1088/1748-6041/11/5/055002.
[28] A. Blaeser, D.F. Duarte Campos, U. Puster, W. Richtering, M.M. Stevens, H. Fischer, Controlling shear stress in 3D bioprinting is a key factor to balance printing resolution and stem cell integrity, Adv. Healthc. Mater. 5 (2016) 326–333, https://doi.org/10.1002/adhm.201500677.
[29] H.L. Kim, G.Y. Jung, J.H. Yoon, J.S. Han, Y.J. Park, D.G. Kim, M. Zhang, D.J. Kim, Preparation and characterization of nano-sized hydroxyapatite/alginate/chitosan composite scaffolds for bone tissue engineering, Mater. Sci. Eng. C. 54 (2015) 20–25, https://doi.org/10.1016/j.msec.2015.04.033.
[30] W.P. Voo, B.B. Lee, A. Idris, A. Islam, B.T. Tey, E.S. Chan, Production of ultra-high concentration calcium alginate beads with prolonged dissolution profile, RSC Adv. 5 (2015) 36687–36695, https://doi.org/10.1039/c5ra03862f.
[31] H. Gheisari, E. Karamian, M. Abdellahi, A novel hydroxyapatite -Hardystonite nanocomposite ceramic, Ceram. Int. 41 (2015) 5967–5975, https://doi.org/10.1016/j.ceramint.2015.01.033.
[32] Q.L. Loh, C. Choong, Three-dimensional scaffolds for tissue engineering applications: role of porosity and pore size, Tissue Eng. - Part B Rev. 19 (2013) 485–502, https://doi.org/10.1089/ten.teb.2012.0437.
[33] J. Yan, Y. Miao, H. Tan, T. Zhou, Z. Ling, Y. Chen, X. Xing, X. Hu, Injectable alginate/hydroxyapatite gel scaffold combined with gelatin microspheres for drug delivery and bone tissue engineering, Mater. Sci. Eng. C. 63 (2016) 274–284, https://doi.org/10.1016/j.msec.2016.02.071.
[34] B. Thavornyutikarn, N. Chantarapanich, K. Sitthiseripratip, G.A. Thouas, Q. Chen, Bone tissue engineering scaffolding: computer-aided scaffolding techniques, Prog. Biomater. 3 (2014) 61–102, https://doi.org/10.1007/s40204-014-0026-7.
[35] J. Jia, D.J. Richards, S. Pollard, Y. Tan, J. Rodriguez, R.P. Visconti, T.C. Trusk, M. J. Yost, H. Yao, R.R. Markwald, Y. Mei, Engineering alginate as bioink for bioprinting, Acta Biomater. 10 (2014) 4323–4331, https://doi.org/10.1016/j.actbio.2014.06.034.
[36] M. Du, W. Song, Y. Cui, Y. Yang, J. Li, Fabrication and biological application of nano-hydroxyapatite (nHA)/alginate (ALG) hydrogel as scaffolds, J. Mater. Chem. 21 (2011) 2228–2236, https://doi.org/10.1039/c0jm02869j.
[37] T. Chae, H. Yang, V. Leung, F. Ko, T. Troczynski, Novel biomimetic hydroxyapatite/alginate nanocomposite fibrous scaffolds for bone tissue regeneration, J. Mater. Sci. Mater. Med. 24 (2013) 1885–1894, https://doi.org/10.1007/s10856-013-4957-7.
[38] A.J. Engler, S. Sen, H.L. Sweeney, D.E. Discher, Matrix Elasticity Directs Stem Cell Lineage Specification, Cell 126 (2006) 677–689, https://doi.org/10.1016/j.cell.2006.06.044.
[39] J. Gopinathan, I. Noh, Recent trends in bioinks for 3D printing, Biomater. Res. 22 (2018), https://doi.org/10.1186/s40824-018-0122-1.